Catalysis Science & Technology

PAPER

View Article Online
View Journal | View Issue

Cite this: *Catal. Sci. Technol.*, 2014, 4, 3306

Ammoxidation of 2-methylpyrazine to 2-cyanopyrazine over Nb–V oxides: marked effect of the Nb/V ratio on the catalytic performance

Naresh Dhachapally,[ab] V. Narayana Kalevaru*[b] and Andreas Martin[b]

Received 4th April 2014,
Accepted 13th June 2014

DOI: 10.1039/c4cy00404c

www.rsc.org/catalysis

A series of bulk Nb–V-containing mixed oxide catalysts with varying Nb/V ratios were synthesized and studied by various solid-state characterization methods. Their catalytic performance was evaluated for the gas phase ammoxidation of 2-methylpyrazine (MP) to 2-cyanopyrazine (CP) that has received growing interest in the chemical industry, recently. The catalysts were characterised by BET-SA, XRD, UV-vis DRS, FTIR, XPS, and TEM. The BET surface area decreased continuously with increase in vanadia content. XRD data confirmed the changes in the crystalline phases with altering Nb/V ratios. UV-vis DRS and FTIR spectroscopic results showed the formation of various kinds of V-oxide species in the catalysts with change in V content. An increase in the concentration of vanadium changes the nature of VO_x species from isolated vanadia species to polymeric vanadia species and then to crystalline vanadia species. Among all the catalysts, the Nb–V–O catalyst with a Nb/V ratio of 1 exhibited the best performance in the ammoxidation reaction (*i.e.* X-MP ~100% and selectivity to 2-CP ~70%). Additionally, a very high space–time yield of CP (>440 g_{CP} kg_{cat}^{-1} h^{-1}) could be successfully achieved. This best catalyst sample revealed two-dimensional polymeric V-oxide species. TEM and SEM showed the formation of a rod-shaped nanoparticle morphology. XPS data revealed that the vanadium is present in two oxidation states (V^{5+} and V^{4+}) in the fresh catalyst (Nb/V = 1) and only one oxidation state (V^{5+}) in the spent catalyst.

1 Introduction

The heterogeneously catalyzed ammoxidation of olefins, aromatics and hetero aromatics is an industrially important process for the manufacture of various commercially useful nitriles, *e.g.*[1] For instance, 2-cyanopyrazine (CP), which is also prepared by the ammoxidation of 2-methylpyrazine (MP), is a valuable intermediate for the production of pyrazinamide, an effective "anti-tubercular drug".[1–6] According to a World Health Organization (WHO) report published in 2012,[7] tuberculosis (TB) still remains an immense global problem. The report claims that there were approximately 8.7 million new cases of TB in 2011 and about 1.4 million deaths across the globe. Geographically, the burden of TB is the highest in Asia and Africa. In fact, India and China together account for about 40% of the world's TB cases. The Millennium Development Goal of WHO is to prevent a TB epidemic by 2015. In view of this, there is a need for developing new and efficient drugs and drug intermediates (for instance, pyrazinamide and cyanopyrazine fall in this category) to handle the TB problem worldwide.

In general, mixed metal oxide (bulk or supported) catalysts are an important class of catalytic materials that are normally employed in numerous oxidation and ammoxidation studies including large-scale industrial applications, *e.g.* ref. 8–13. Different catalytic systems for the ammoxidation of MP to CP have been investigated so far, and among them V-based catalysts are found to be the most promising ones.[1,3–6,14–20] In addition, $FePO_4$,[21] MoVPO,[16] VPO-based solids,[22] heteropolyacids,[17,23] $VMoO_x$ (ref. 24) and supported catalysts such as V_2O_5/TiO_2 (ref. 3, 4 and 25) are some of the interesting catalyst systems for the ammoxidation of MP to CP. Furthermore, a couple of decades ago some other studies were also focused on the reaction kinetics using Sb–V–Mn mixed oxides, *e.g.* ref. 26. One of the main disadvantages of the reported catalysts, *e.g.* ref. 3, 6, 16 and 17, is that they reveal rather low space–time yields of CP (STY-CP) and their relatively low stability. Therefore, the development of efficient catalysts for the target reaction is the focus of the present research.

In the recent past, Nb-containing catalyst systems have also been reported to be effective and attractive and hence much attention is being focused on the application of Nb oxides for various selective oxidation reactions.[27,28] However,

[a] *Begumpet, Doulthabad, Medak, Andhrapradesh, India-502334*
[b] *Leibniz-Institut für Katalyse e.V. an der Universität Rostock, Albert-Einstein-Str. 29a, D-18059 Rostock, Germany. E-mail: narayana.kalevaru@catalysis.de; Fax: +49 381 128151284; Tel: +49 381 1281284*

niobia itself is a poorly active solid for different catalytic reactions, but the combination of niobium oxide with other redox components (*e.g.* vanadium, chromium, molybdenum *etc.*) could significantly improve both the activity and selectivity of many important oxidation reactions. More particularly, the combination of vanadium and niobium oxides has been found to be highly selective and also active for different oxidation and ammoxidation reactions.[14,29–32] In this context, the synthesis and application of Nb–V-containing oxide materials for the present ammoxidation of MP to CP could be helpful.

Recently we have observed that bulk metal vanadates are very active and selective for the present MP ammoxidation. Furthermore, these catalytic systems also offer a very high STY-CP.[33–35] Particularly, a Nb–V–O catalyst has shown a better performance compared to other metal vanadates in the ammoxidation of MP to CP.[33,34] The key point to reach high catalytic performance appears to be the ability to tune the catalyst surface and bulk structure by changing different characteristics of the solids. For example, this can be accomplished by optimizing the ratio of the active components (*i.e.* Nb and V) in the catalyst composition.

The main objective of the present study is to prepare various Nb–V-containing mixed oxide catalysts with varying Nb/V ratios and evaluate its impact on the catalytic performance in the gas phase ammoxidation of MP to CP. A further intention of this investigation is also to obtain a comprehensive understanding of the physico-chemical characteristics of the catalyst materials by applying various characterization techniques.

2 Experimental

2.1 Catalyst preparation

The preparation of the bulk Nb–V–O catalysts was carried out in two steps. The 1st step dealt with the preparation of a niobium metal solution using the requisite quantities of the ammonium niobium oxalate (ANO) precursor. ANO was dissolved in distilled water, to which a desired amount of citric acid (mole ratio of metal : citric acid = 3 : 1) was added, and then the mixture was stirred at room temperature until a clear solution was obtained. The 2nd step contained the preparation of a vanadium solution using NH_4VO_3 (AMV) as a precursor for vanadium. The required amount of AMV was taken in distilled water and a suitable amount of oxalic acid (OA) was added to it (mole ratio of AMV : OA = 1 : 1.5). The above solution was then heated to 60 °C on a hotplate and then the solution was kept at the same temperature for 10 minutes under stirring. The vanadium solution turned a dark blue color after the addition of oxalic acid. Afterwards, the above vanadium–oxalic acid solution was added dropwise to the niobium–citric acid solution at 60 °C under constant stirring. After complete addition, the mixture was heated to 80 °C and then slowly evaporated to dryness on a hotplate. The solid thus obtained was further dried at 110 °C for 16 h in an oven. Finally, the samples were calcined at 500 °C for 12 h in air (4 l h^{-1}). Using the same procedure, a series of Nb–V–O solids was prepared with varying Nb/V ratios in the range of 0.9/0.1 to 0.1/0.9. Additionally, pure V_2O_5 was prepared by direct calcination of the AMV precursor at 500 °C for 4 h in air (4 l h^{-1}). Similarly, the pure Nb_2O_5 was also prepared by direct calcination of the ANO precursor at 500 °C for 4 h in air (4 l h^{-1}). The sample denotation and the Nb/V ratios are given in Table 1.

2.2 Catalyst characterization

The X-ray diffraction (XRD) patterns were obtained with an X-ray diffractometer STADIP (Stoe, Darmstadt, Germany) using Ni-filtered CuKα radiation (λ = 1.5418 Å). The crystalline phases were identified by referring to the ASTM data files.

The pore size distribution (PSD) and surface areas (BET-SA) of the catalysts were determined using a NOVA 4200e instrument by N_2-physisorption at −196 °C. Prior to the measurements, the known amount of catalyst was evacuated for 2 h at 200 °C to remove physically adsorbed water. The pore size distribution (PSD) was calculated by BJH methodology using the data from the desorption branch. We have taken 49 points in total for this measurement (*i.e.* 25 adsorption and 24 desorption points) in the P/P_0 range of 0.05 to 0.98. All of these parameters were calculated using the software "NovaWin version 11.03" provided by Quantachrome Instruments.

Scanning Electron Microscopy (SEM) measurements were performed using a JSM-7401F apparatus (Jeol) with a 1.0 nm resolution at an accelerating voltage of 15 kV. To prepare samples for SEM, samples were adsorbed on a silicon wafer and allowed to dry in air overnight. Transmission electron microscopy (TEM) analysis was performed by using a JEM-2100F (Jeol) high-resolution transmission electron microscope (HRTEM) at a voltage of 200 kV. The catalyst was suspended in an ethanol medium under ultrasonication at room temperature for 10 min. A drop of the suspension was placed on a carbon-coated copper grid. After drying the grid, the sample was inserted in the TEM instrument for analysis.

The UV-vis diffuse reflectance spectra (DRS) were recorded with an Avaspec-2048 (Avantes) instrument using a solid probe. For the correction of baseline $BaSO_4$ (spectroscopic grade) was used as a reference material.

FTIR spectra were recorded with a Bruker Alpha spectrometer (IFS 66) using a solid probe. For these experiments, the catalyst powder was pressed into self-supporting discs (50 mg, Ø 20 mm). Before the measurement, the samples were

Table 1 Sample denotations and Nb/V ratios of various Nb–V–O catalysts

Sample denotation	Catalyst composition, Nb/V ratio (mol)
1Nb0VO	1 : 0
9Nb1VO	9 : 1
3Nb1VO	3 : 1
1Nb1VO	1 : 1
1Nb3VO	1 : 3
1Nb9VO	1 : 9
0Nb1VO	0 : 1

pre-treated or dehydrated by heating in helium up to 400 °C for 10 min and then cooled down to room temperature followed by evacuation. Generally, the spent samples were also degassed before measurement.

The X-ray photoelectron spectroscopic (XPS) measurements were done with a VG ESCALAB 220iXL unit using MgKα radiation (E = 1253.6 eV) at a base pressure of the UHV chamber. The C1s binding energy (BE) of 284.6 eV was used as a reference for the determination of the binding energies.

2.3 Catalytic tests

The catalytic tests were performed in a down-flow fixed-bed stainless steel reactor (i.d. = 9.4 mm, length = 250 mm) in vapor phase at atmospheric pressure. In a typical experiment, 1 g of the catalyst particles (0.5–0.8 mm size) diluted with equal amounts of corundum (catalyst : corundum = 1 : 1 w/w) having the same size were loaded into the reactor. The catalyst was packed between two quartz wool plugs in the middle of the reactor. Also the upper and lower portions of the catalyst bed were filled with corundum. The liquid feed of the premixed MP and H_2O mixture (mole ratio of MP : H_2O = 1 : 13) was metered using a HPLC pump. The liquid was vaporized in a preheating zone. The flow rates of gases such as NH_3, air and N_2 were controlled by mass flow controllers. These gases were taken from commercially available compressed gas cylinders (Air Liquide). The molar ratio of the reactant feed mixture was set to MP : H_2O : NH_3 : air : N_2 = 1 : 13 : 7 : 26 : 22. The reaction was carried out in the temperature range of 360–400 °C, GHSV = 9500 h^{-1} and τ = 0.37 s. Two thermocouples were positioned: one was positioned at the center of the catalyst bed to indicate the reaction temperature, and the other one was attached to the furnace through a temperature indicator-cum-controller to steer the temperature of the reactor. The product samples were collected every hour under steady state conditions and analyzed off-line with a gas chromatograph (GC-2014 Shimadzu, Japan) equipped with a flame ionization detector (FID). The liquid samples were analyzed using an FFAP column, while the gaseous products (*i.e.* CO and CO_2) were also analyzed with the same GC using a methanizer and a GSQ column.

Conversion (X-MP) of MP, yield (Y-CP) and selectivity (S-CP) of CP were calculated by the following formulas:

$$\text{X-MP} = \frac{\text{number of moles of MP reacted}}{\text{number of moles of MP fed}} \times 100\%$$

$$\text{Y-CP} = \frac{\text{number of moles of CP formed}}{\text{number of moles of MP fed}} \times 100\%$$

$$\text{S-CP} = \frac{\text{number of moles of CP formed}}{\text{number of moles of MP reacted}} \times 100\%$$

The yield and selectivity of the main byproducts pyrazinamide and pyrazine as well as the carbon oxides were calculated in the same way. The space–time yield of CP (STY-CP) was calculated using the following equation:

$$\text{STY-CP} = \frac{\text{CP formed}\left[\text{g h}^{-1}\right]}{\text{catalyst amount}\left[\text{kg}\right]}$$

3. Results and discussion

3.1 XRD

The XRD patterns of the fresh catalysts with varying Nb/V mole ratios are depicted in Fig. 1. The lattice parameters are presented in Table 2. The obtained patterns clearly show that the type of crystalline phase formed depends strongly on the Nb/V ratio applied.[29–31] The XRD reflections of the as-synthesized niobia (1Nb0VO sample) at 2θ = 22.60, 28.58, 36.70, 46.23 and 50.67° clearly point to the crystalline Nb_2O_5 phase, as expected. It is known from the literature that niobia crystallizes in several phases[36,37] and the pattern found in the present case is very similar to that of the TT-phase of Nb_2O_5 (JCPDS-ICDD file 27-1312), which is reported to be stable up to 700 °C. In the present study, 500 °C is the calcination temperature used and hence the TT-phase should be stable in these samples. The 0Nb1VO sample shows reflections at 2θ = 15.39, 21.31 (100%), 21.74, 26.20, 30.07, 32.43 and

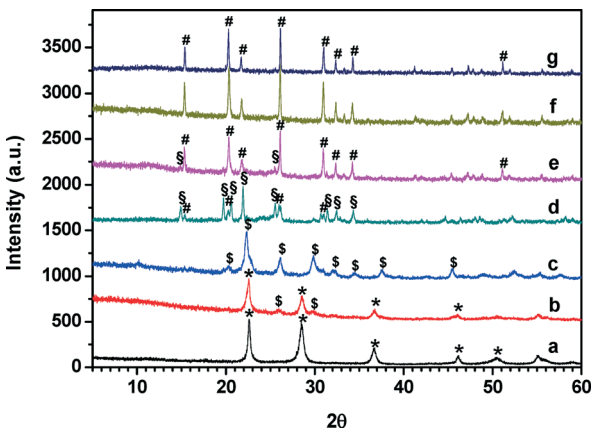

Fig. 1 XRD patterns of fresh Nb–V–O catalysts (* = Nb_2O_5 (JCPDS-ICDD file 28-0317); $ = $Nb_{18}V_4O_{55}$ (JCPDS-ICDD file 46-0087); § = $NbVO_5$ (JCPDS-ICDD file 46-0046); # = V_2O_5 (JCPDS-ICDD file 86-2248)) (a – 1Nb0VO, b – 9Nb1VO, c – 3Nb1VO, d – 1Nb1VO, e – 1Nb3VO, f – 1Nb9VO, g – 0Nb1VO).

Table 2 Lattice parameters of various Nb–V–O catalysts

Catalyst	System	d^a (Å)	Lattice parameters (Å)			Volume (Å^3)
			a_0	b_0	c_0	
1Nb0VO	Hexagonal	3.93	3.607	—	3.925	44.2
9Nb1VO	Hexagonal	3.93	3.607	—	3.925	—
3Nb1VO	Orthorhombic	3.96	7.939	17.310	17.610	242.0
1Nb1VO	Orthorhombic	4.05	11.860	5.514	6.915	452.4
1Nb3VO	Orthorhombic	4.39	11.500	4.369	3.557	—
1Nb9VO	Orthorhombic	4.39	11.500	4.369	3.557	—
0Nb1VO	Orthorhombic	4.39	11.500	4.369	3.557	178.8

[a] 100% peak.

34.36°, which is a typical pattern of the V_2O_5 phase (JCPDS-ICDD file 86-2248, Shcherbinaite). The other samples exhibit patterns that correspond well to various Nb–V–O mixed oxides. Besides the Nb_2O_5 phase, the 9Nb1VO sample reveals reflections caused by the Nb-rich $Nb_{18}V_4O_{55}$ mixed oxide phase (JCPDS-ICDD file 46-0087). The XRD pattern of the 3Nb1VO sample shows a single phase of $Nb_{18}V_4O_{55}$ mixed oxide with peaks at 2θ = 20.11, 22.38 (100%), 26.21 and 29.70°, which is approximately balanced by the stoichiometry used for the preparation of this sample. The XRD data of the 1Nb1VO sample show major peaks at 2θ = 14.90, 19.69, 20.54, 21.90 (100%), 25.53 and 25.94° pointing to the formation of the $NbVO_5$ mixed oxide phase (JCPDS-ICDD file 46-0046). However, besides the formation of $NbVO_5$, a very small amount of $Nb_{18}V_4O_{55}$ (shoulder peak at 2θ = 22°) is still detected in this solid. In addition, very weak reflections belonging to V_2O_5 are already observed at 2θ = 15.37, 20.29 and 26.15°. The XRD pattern of the 1Nb3VO sample mainly shows crystalline V_2O_5 (JCPDS-ICDD file 86-2248, Shcherbinaite) due to the higher concentration of vanadium in this sample. However, a couple of weak reflections corresponding to crystalline $NbVO_5$ are also still detected at 2θ = 14.90 and ~26°. Due to the much higher vanadium proportion, the 1Nb9VO sample exclusively reveals the formation of crystalline V_2O_5; no reflections of any mixed Nb–V–O phase or pure Nb_2O_5 can be seen.

Furthermore, the XRD patterns of the spent catalysts were found to be similar to those of the fresh catalysts; therefore, they are not shown here. This result implies that the catalysts are quite stable during the course of the reaction with respect to their phase composition.

3.2 BET surface areas, adsorption isotherms and pore size distribution

The specific surface areas of the studied oxide catalysts are displayed in Table 3. The surface area of pure Nb_2O_5 (1Nb0VO sample) is 86 $m^2\ g^{-1}$ while the surface area of pure V_2O_5 (0Nb1VO sample) is only 4 $m^2\ g^{-1}$. However, a drastic drop in the surface area is observed with the decrease in the Nb/V ratio (*i.e.* increase in vanadium content) of the solids up to the 1Nb1VO sample and then this decrease is not much affected with further increase in V content due to increased concentration of vanadia, which has a low surface area. This obviously demonstrates that the vanadium ions might be increasingly blocking the pores of niobium oxide; they are probably occupying interstitial positions of the host matrix or less porous phases are formed. The latter is supported by the above discussed XRD analyses. The pore volumes are also observed to obey the same trend as that of surface areas. Surface areas of the spent samples were also measured (see Table 3). Their surface areas were found to be marginally decreased compared to those of the fresh catalysts pointing again to only small changes. Furthermore, the average pore size estimated in both the fresh and spent samples is also presented in Table 3.

The adsorption isotherms of both the fresh and spent Nb–V–O catalysts are given in Fig. 2A and B. One can notice that the nature of adsorption isotherm in sample a (pure Nb_2O_5) is of type IV and V, which is typical for mesoporous solids.[38,39] With increasing vanadium content, the hysteresis shapes are changing from types IV and V to types II and III, which belong to non-porous solids. Such a phenomenon is also evidenced from the drastic decrease in their surface areas when V content is increased (see Table 3). It can be concluded that the pore structure of the catalysts is changing from mesoporous to non-porous as a function of vanadium content. The hysteresis of 0Nb1VO almost looks like a straight line, indicating its non-porous nature. Consequently, this solid

Table 3 BET surface areas and pore volumes of the Nb–V–O catalysts with varying Nb/V ratios

	Surface area ($m^2\ g^{-1}$)		Pore volume (ml g^{-1})		Average pore size (nm)	
Catalyst	Fresh	Spent	Fresh	Spent	Fresh	Spent
1Nb0VO	86	—	0.193	—	2.7	—
9Nb1VO	39	37	0.139	0.138	3.7	3.4
3Nb1VO	16	13	0.101	0.098	10.7	10.5
1Nb1VO	8	7	0.088	0.060	18.0	20.0
1Nb3VO	7	6	0.060	0.050	>20	>20
1Nb9VO	6	8	0.047	0.048	>20	>20
0Nb1VO	4	—	0.049	—	>20	>20

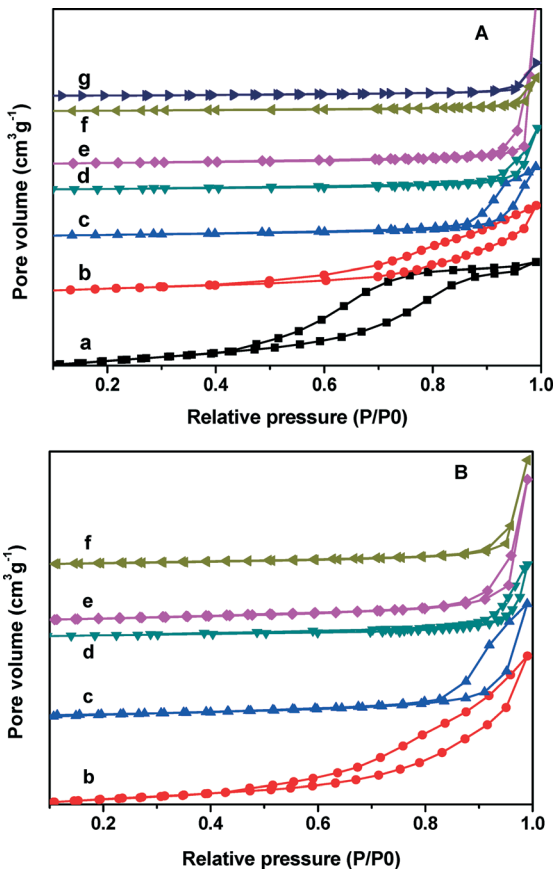

Fig. 2 Adsorption isotherms of various Nb–V–O catalysts (A: fresh catalysts, B: spent catalysts; sample denotation as that of Fig. 1).

exhibited the lowest surface area. The isotherms of the spent catalysts (Fig. 2B) appeared almost similar pointing to no significant pore structure change during the course of the reaction.

The pore size distributions of both fresh and spent Nb–V–O catalysts with varying Nb/V ratios are shown in Fig. 3A and B. Obviously, all samples revealed a unimodal pore size distribution. The 1Nb0VO sample showed a sharp and high intensity peak at around 2.7 nm pointing to the exclusive presence of mesopores. After incorporation of certain amounts of vanadium, the dominant pore diameter of the 9Nb1VO sample moved slightly towards a higher pore range, *i.e.* at 4 nm. At the same time, the intensity of the pore volume curve is also decreased considerably in comparison with the vanadium-free solid proving a considerably changed pore structure and surface area due to the already discussed effects of vanadium introduction. In Fig. 3A one can also notice that the pore diameter of the other samples with further increasing vanadium content is shifted to higher values and thereby decreases the surface area of the solids dramatically. In the catalysts having higher V contents the pore structure of the catalysts seemed to be almost collapsed and such catalysts show a similar behavior as that of pure V_2O_5 showing just a straight line. The pore size distribution of the spent catalysts (Fig. 3B) is found to be similar to their corresponding fresh catalysts; the intensity of the pore volume curve is decreased slightly and hence their surface areas are a little bit decreased. The pore volumes and pore diameters of Nb–V–O oxide catalysts are given in Table 3.

3.3 SEM and TEM

The SEM image of the 1Nb1VO sample (Fig. 4A) clearly shows the formation of bundles of rod-shaped Nb–V–O small particles. In the image, one can also see (inset) the rods with several hundreds of nanometer length. A TEM image is presented in Fig. 4B clearly showing the formation of rod-shaped and also some needle-like nanoparticles in the catalyst. The rod-shaped nanoparticles seem to be major in proportion, which are more likely related to the $NbVO_5$ phase, while the small proportion of the needle-like morphology is typical for V_2O_5 nanoparticles.

3.4 UV-vis DRS

The UV-vis diffuse reflectance spectra of fresh and spent samples recorded at room temperature are presented in Fig. 5A and B. The LMCT (ligand-to-metal charge transfer) bands are a sensitive indicator for the vanadium coordination and the degree of

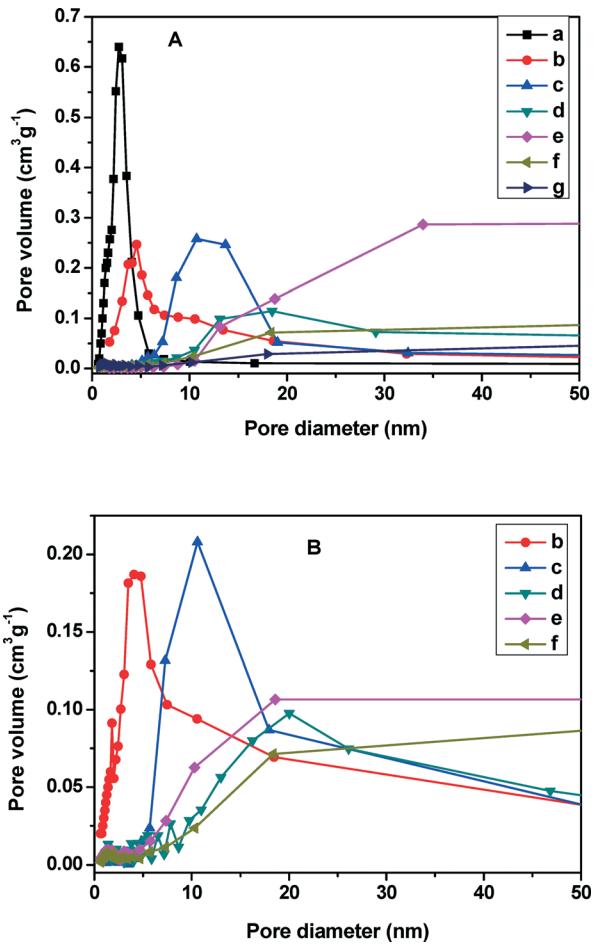

Fig. 3 Pore size distribution of various Nb–V–O catalysts (A: fresh catalysts, B: spent catalysts; sample denotation as that of Fig. 1).

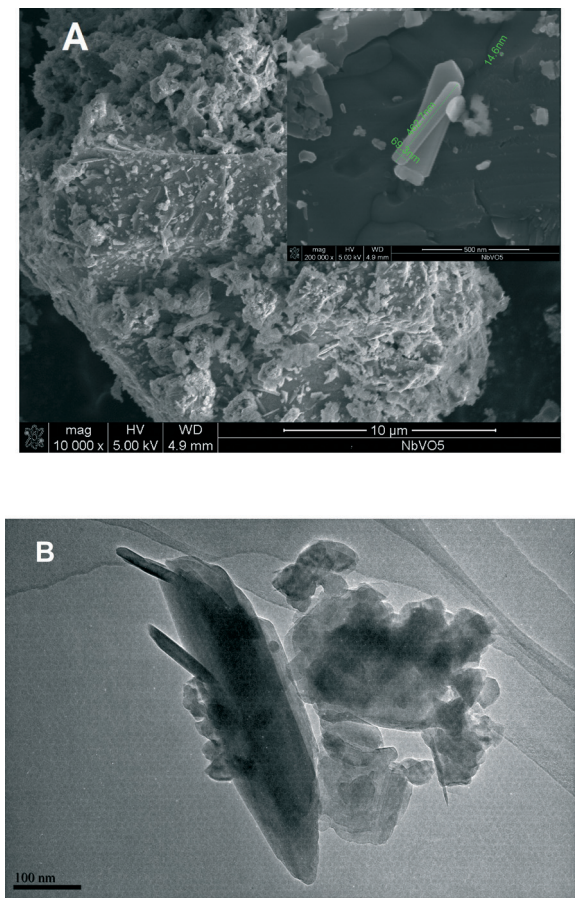

Fig. 4 Electron microscopy images of 1Nb1VO sample (Nb/V = 1) (A: SEM, B: TEM)

polymerization of the vanadium species. The local structures of the V^{5+} cations are often associated with the band positions of the LMCT transitions. In the literature, many research groups have studied thoroughly the CT band energies of vanadia-based catalysts and these are lying in between 200 and 570 nm. CT bands lying in between the 420 and 560 nm regions are characteristic of crystalline VO_x species in a distorted octahedral environment while the bands in the range of 270–400 nm regions are characteristic of oligomeric tetrahedral coordination of V^{5+} ions. The bands around the 412 nm region are specific to square pyramidal V^{5+} ions and the bands that appeared <300 nm are typical for CT transitions of isolated (monomeric) tetrahedrally coordinated V^{5+} ions and also V^{4+} and V^{3+} ions.[40,41] Generally, CT transitions are more intense than the d–d transitions in metal oxides.

The measured spectra of the present samples showed three broad absorption bands in the range of 550–420, 420–270 and below 270 nm. The 1Nb0VO sample showed only two band maxima at 330 and 260 nm, which belong to the LMCT transitions of pure Nb_2O_5. Similarly, all other samples of the present study exhibited three absorption bands with band maxima at 235, 340 and 480 nm (see Fig. 5A). In the 9Nb1VO sample, only polymeric (330 nm) and isolated VO_x species (235 nm) of V^{5+} ion bands were clearly observed, which are due to the highly dispersed nature of VO_x species (due to the presence of low vanadium content). However, the band intensities increased with increase in vanadium content. The bands in the 0Nb1VO sample correspond well to the CT transitions of V^{5+} ions (*i.e.* pure V_2O_5). The spectra of samples from 3Nb1VO to 1Nb9VO with increasing vanadium content have shown bands that are quite similar to those of pure V_2O_5; however, the band positions and energies are quite different from bulk V_2O_5. The transition energies of vanadium ions are also found to vary with the Nb/V ratio of the catalyst. It seems that the metal incorporation plays an important role on the structure in the formation of different nature and coordination environments of VO_x species. Such changes in the nature of VO_x species formed are also expected to exhibit clear impact on the catalytic performance.

The spectra of the spent catalysts are very similar to the fresh ones. This could be assigned to the stability of the crystalline phases that seem to be not altered during the course of the reaction. These results are well correlated with the results obtained by phase and texture analysis.

3.5 FTIR spectra

The FTIR spectra of fresh Nb–V mixed oxide solids are shown in Fig. 6A. Pure vanadia (0Nb1VO) and niobia (1Nb0VO) reveal the well-known spectra and are not shown here. V_2O_5 generally exhibits two characteristic bands: one at *ca.* 1020 cm^{-1}, (stretching vibrations of V^{5+}═O bonds) and a second broad one at *ca.* 835 cm^{-1} (V–O–V deformation vibrations). Nb_2O_5 shows four broad bands at *ca.* 850, 725, 635 and 500 cm^{-1}. These bands can be assigned to Nb═O in highly distorted NbO_6 groups, symmetric stretching of the niobium polyhedra, and ν(Nb–O) in slightly distorted NbO_6 octahedra, respectively.

The spectrum of the 9Nb1VO sample exhibits various bands at 1020, 975, 885, 735, 575 and 475 cm^{-1}. The bands at 885, 735, 575 and 475 cm^{-1} can be assigned to the Nb_2O_5 matrix. The band at 1020 cm^{-1} is due to the stretching vibrations of the V═O bonds, probably belonging to microcrystalline V_2O_5 that is present in the sample, even at such a low vanadium content.[12,32,42] As expected, the intensity of this band is increasing significantly with increase in V contents of the

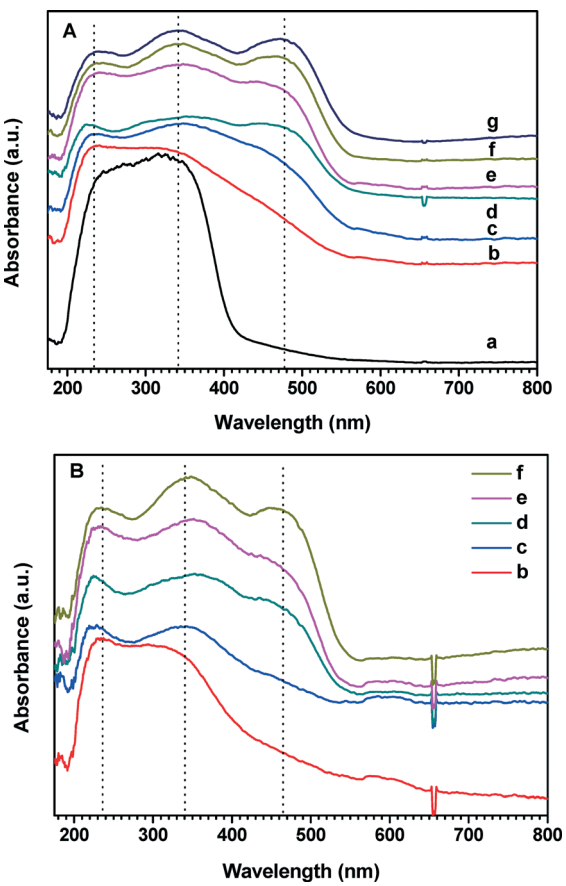

Fig. 5 UV-vis DRS spectra of various Nb–V–O catalysts (A: fresh catalysts, B: spent catalysts; sample denotation as that of Fig. 1).

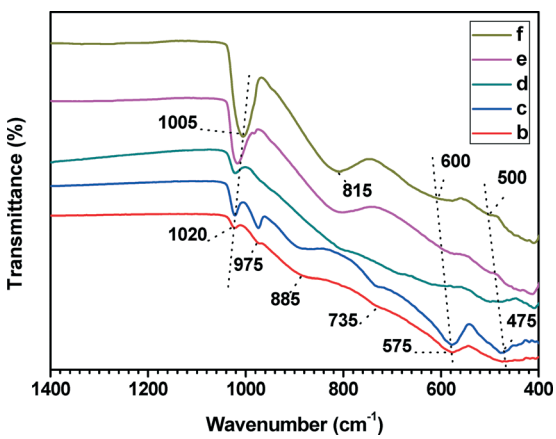

Fig. 6 FTIR spectra of various Nb–V–O catalysts (sample denotation as that of Fig. 1)

catalysts. Another band observed at 975 cm^{-1} could be assigned to the two-dimensional amorphous vanadium oxide species present in the system. This band has also been correlated with the vibrations of isolated V=O bands of the type VO^{2+}. Moreover, the band at 975 cm^{-1} may also be due to the bulk V=O functionality of the crystalline $Nb_{18}V_4O_{55}$ phase. When the vanadium content increases, the band becomes broadened and shifts to lower frequencies, which indicates a weakening of the $(V=O)^{3+}$ bonding coincident with an amorphous oxide phase or the presence of neighboring V^{4+} ions. Interestingly, the band at 975 cm^{-1} almost disappeared at higher vanadium contents, which means that the bulk V_2O_5 portion has also increased, and perhaps this band is overlapped by the intense and relatively broad band that appeared at 1005 cm^{-1}. In addition, the band at 885 cm^{-1} also vanished, which is due to the decline of the niobia proportion. The band that appeared at 1005 cm^{-1} is certainly due to stretching vibrations of V=O bands for V_2O_5,[13] while the band at 815 cm^{-1} is due to bending vibrations of V–O–V groups in $NbVO_5$ (asymmetric stretching of VO_4^{3-} entity). The broadening of these bands with vanadia loading indicates a stronger interaction between vanadia and niobium species. Furthermore, the formation of the orthovanadate phases at higher loadings may be due to the interaction of the isolated vanadate species with the host matrix. These results are in good agreement with the literature reports[12,32,41] revealing that the stabilization of vanadate species depends on the nature of acid–base properties of the host matrix and also on the vanadia concentration. No considerable differences could be noticed between the fresh and spent samples again; thus, the spectra of the spent samples were not included.

3.6 XPS

The Nb $3d_{5/2}$ BEs of the best (fresh and spent) 1Nb1VO sample (206.9 and 207.3 eV, respectively) are given in Table 4. This region is assigned to Nb^{5+} ions matching well with the data reported in the literature.[43,44] XP spectra of the fresh and spent (the best) 1Nb1VO catalyst is given in Fig. 7. The V $2p_{3/2}$ spectra of fresh catalyst can be fitted into two components.[45,46] The one at higher binding energy (518.0 eV) is assigned to the V^{5+} sites. The second peak at lower binding energy (516.6 eV) can be related to the presence of certain amounts of V^{4+} species in the near-surface region. Amarilla *et al.*[44] also claimed the formation of V^{4+} species (about 25%) in $NbVO_5$ being isostructural to monophosphate tungsten bronzes. However, in the used catalyst, only V^{5+} (BE = 517.4 eV) ions were detected. The O1s spectra showed a peak at around 530.1 eV, which is attributed to the O^{2-} ion in $NbVO_5$. In addition

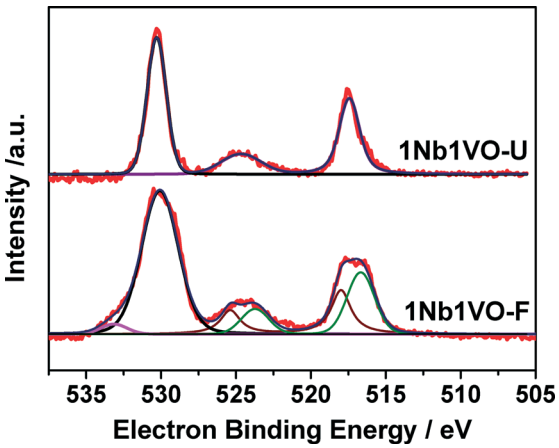

Fig. 7 XP spectra of the best (fresh and spent) 1Nb1VO catalyst (F = fresh catalyst, U = used catalyst, sample denotation as that of Fig. 1).

to the main peak, a very small shoulder appeared at 533.2 eV in the spectra and the contribution of this peak is only less than 5%. The weak peak might be related to the oxygen attached to the lattice or surface defects in the $NbVO_5$ structure.[47] However in the spent catalyst, only a single type of oxygen species was observed.

The nominal value of the atomic ratio of Nb/V in this catalyst is 1. Interestingly, the Nb/V ratio in the near-surface region is found to be different. The fresh catalyst exhibits a Nb/V ratio of 0.79, while the spent catalyst displays 0.62 (see Table 4). In any case, there is a clear enrichment of vanadium in the near-surface region compared to its bulk value. Such enrichment is more pronounced in the case of a spent catalyst. This fact shows that reaction conditions have shown a certain influence on the migration of V-species from the bulk to the surface during the course of the reaction. Nonetheless, no considerable difference in the bulk Nb/V ratio (estimated from ICP) could be noticed between the fresh and spent catalyst.

3.7 Catalytic results

The effect of the reaction temperature on the conversion of MP (X-MP), yield of CP (Y-CP) and selectivity to CP (S-CP) is displayed in Fig. 8A–C. The conversion of MP is increased with increase in temperature from 360 °C to 380 °C where nearly the total conversion is reached in most cases and hence it remained more or less constant at this level with further rise in temperature to 400 °C. As expected, the 1Nb0VO sample exhibited a very low activity (X-MP ≤20%) and selectivity (S-CP ~5%) at any given reaction temperature. Pyrazine

Table 4 XPS results of the best (fresh and spent) Nb–V–O catalyst with Nb/V = 1

Catalyst	Nb^{5+}		V^{5+}		V^{4+}		O		O		Nb/V
1Nb1VO	BE (eV)	at.%	BE (eV)	at.%	BE (eV)	at.%	BE (eV)	at.%	BE (eV)	at.%	ratio[a]
Fresh	206.9	8.5	518.0	4.7	516.6	6.1	533.2	2.2	530.1	45.8	0.79
Spent	207.3	11.1	517.4	18.0	—	—	—	—	530.3	60.3	0.62

[a] Near-surface region.

(Py) was the main byproduct while pyrazinamide (PyA), small amounts of CO, and CO_2 were the other byproducts of the reaction. Even though the pyrazinamide is formed, it is also a desired product with good commercial application as an anti-tuberculosis drug. In fact, the formed major product CP is also ultimately converted to Py-A by catalytic hydration on an industrial scale in the direction of preparing anti-tuberculosis drug formulations. In general, the selectivity of CP increased with temperature up to 380 °C and then slightly decreased with further increase in temperature. Similarly, the yield of CP also increased (Fig. 8B) with temperature up to 380 °C and then decreased. The best results were obtained over the sample with a Nb/V ratio of 1.

The influence of the Nb/V ratio on the catalytic performance of the solids at 380 °C is shown in Fig. 9. Pure Nb_2O_5 is much less active and not selective for the formation of CP. It can be easily seen that the presence of vanadium shows a remarkable influence on the catalytic performance with respect to the desired reaction. Therefore, both the conversion of MP and the selectivity of CP depend strongly on the Nb/V ratio of the catalysts. In the 9Nb1VO sample, Y-CP reaches only 22% while the yield for pyrazine climbs to 52%. The yield of CP passes through a maximum (Y-CP is close to 70%) over the 1Nb1VO sample with increased vanadium content. However, a further increase in vanadium content reveals an adverse effect despite the conversion remaining high. The obtained yield of CP over pure V_2O_5 was only 54% (0Nb1VO). In addition, the results clearly showed that the sum of the yields of both CP and PyA accounts to nearly 90% using the 1Nb1VO sample whereas increasing or decreasing vanadium contents promotes the formation of unwanted byproducts. Large amounts of pyrazine are formed using catalysts with niobium excess and total oxidation is dominant with increasing vanadium proportion. From these results, it is very clear that Nb/V ratio has a strong influence on the catalytic performance. Consequently, one can notice that the Nb–V–O catalysts with a Nb/V ratio of 1 ($NbVO_5$) exhibit the best performance compared to other solids of this series.

Furthermore, the STY-CP (see Fig. 9) is also increased with an increase in the vanadia content up to a Nb/V ratio of 1 (440 g_{CP} kg_{cat}^{-1} h^{-1}). After reaching this maximum, the STY-CP drops again to *ca.* 350 g_{CP} kg_{cat}^{-1} h^{-1} for pure V_2O_5. However, the aggregated STY for CP plus PyA might reach *ca.* 600 g_{CP+PyA} kg_{cat}^{-1} h^{-1}; this is much higher than the reported literature up to now. The better catalytic performance of Nb–V–O catalysts particularly with a Nb : V ratio of 1 : 1 (*i.e.* 1Nb1VO catalyst) is more likely due to the presence of higher concentrations of the $NbVO_5$ phase in this formulation compared to all other solids having either high niobium or high vanadium contents. At a higher content of Nb, more Nb-oxide or mixed oxide ($Nb_{18}V_4O_{55}$) phases are present while at high vanadium contents mainly V_2O_5 is present. Both these situations and phase composition seem to be not suitable for achieving enhanced catalytic performance. Usually, when V_2O_5 phase is formed, the lattice oxygen is connected through V^{5+}–O–V^{5+} bonds, where it is very easy to remove such

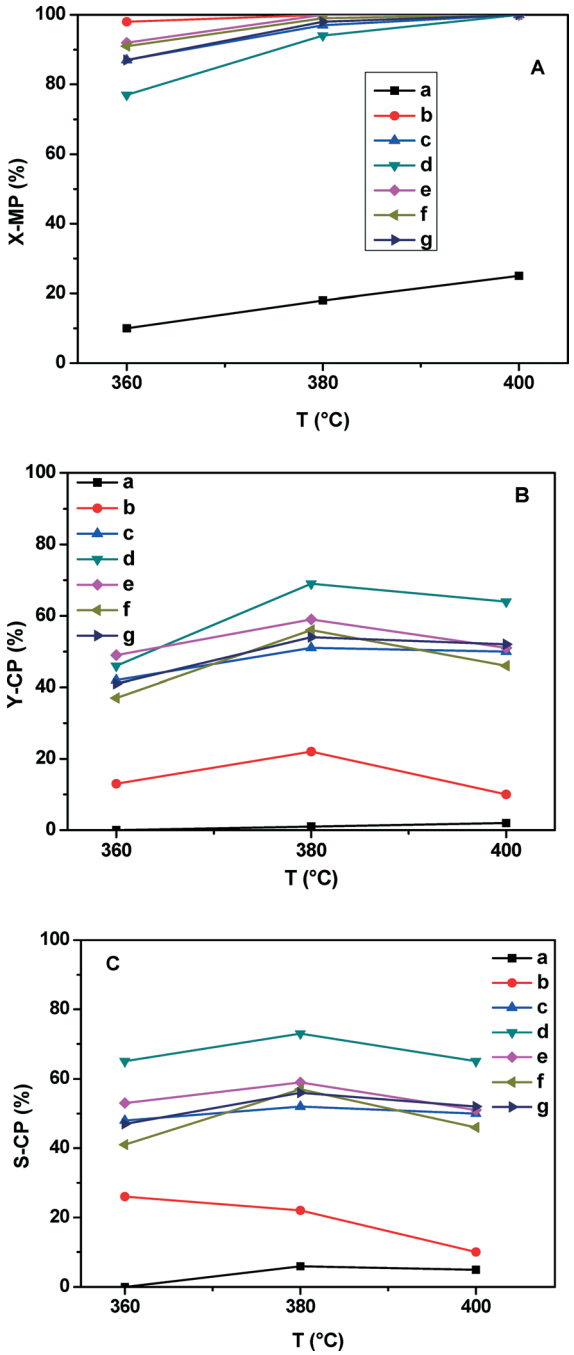

Fig. 8 Effect of temperature on the catalytic performance of various Nb–V–O catalysts (A: conversion of MP; B: yield of CP, C: selectivity to CP) (reaction conditions: MP : H_2O : NH_3 : air : N_2 = 1 : 13 : 7 : 26 : 22; cat. wt. 1 g; sample denotation as that of Fig. 1).

lattice oxygen due to the high reducibility of the two V^{5+} ions, which in turn leads to easy combustion of MP and thus reduced selectivity of the desired product, CP. On the other hand, when metal vanadate is formed (*e.g.* $NbVO_5$ in the present case), the lattice oxygen is present in V^{5+}–O–M^{n+} bonds (M = Nb in the present case) instead of V^{5+}–O–V^{5+} bonds present in the V_2O_5 phase. This situation leads to lower concentrations of V^{5+}–O–V^{5+} bonds and hence low combustion activity of the catalyst compared to V_2O_5. In other words, the high selectivity of the

1Nb1VO catalyst is a result of the fact that the oxide is made up of isolated VO_4 units that are separated from each other by NbO_x units in such a way that all the lattice oxygen ions are located in the solid bridge between V^{5+} and Nb^{+5} ions. Our results are in good agreement with the literature reports that deal with various metal vanadates and claim similar observations to ours.[48–50] Another reason for the improved performance of 1Nb1VO catalyst is the enrichment of both vanadium and niobium species in the near-surface region, as evidenced by XPS (see Table 4). The nominal value of the Nb : V bulk ratio in the as-synthesized catalyst is 0.5 : 0.5 (*i.e.* 1 : 1). However, XPS analysis revealed that the fresh catalyst exhibits a Nb : V ratio of 0.79 : 1 in the near-surface region, while the spent catalyst displays a Nb : V ratio of 0.62 : 1. Nevertheless, further studies are certainly necessary to get deeper insights on deriving structure–activity relationships.

Herein we discuss some important issues related to the nature of active sites required, structure–activity relationships as well as mechanistic aspects reported in the literature using different catalyst systems for the present ammoxidation reaction. Hong *et al.*[16] applied MOVPO catalysts and claimed that the ammoxidation of MP proceeds through a series of dehydrogenation and oxidation steps to form various intermediates such as pyrazinyl aldehyde and pyrazinyl carboxylic acid, which then finally converted into CP. Due to the involvement of dehydrogenation and oxidation steps, the authors suggest that the catalyst should contain both dehydrogenation sites as well as oxygen supply units in appropriate amounts. V_2O_5 is the main active component in the MoVPO catalyst for oxygen supply; however pure V_2O_5 also has a very strong activity of oxygen supply and only a few sites of dehydrogenation. As a result, it promotes over-oxidation of MP and thereby low selectivity of CP. In order to minimize the combustion activity of bulk V_2O_5, they have added P as a promoter so that it can react with V_2O_5 and form $(VO)_2P_2O_7$ and/or α- or β-$VOPO_4$ phases. In these catalysts, V═O is considered to be the site of oxygen supply, and V^{4+} or V^{4+}–P–O is the site of dehydrogenation. The addition of MoO_3 strengthens the ability of oxygen supply as it can connect with V to increase the fluidity of electron and weaken the bond energy of V–O. The authors state that this situation can also change the space structure between sites of dehydrogenation and oxygen supply. Addition of TiO_2 can further stabilize V^{4+}, keep the appropriate V^{4+}/V^{5+} ratio, and also make VO_x species more dispersed on the surface of the catalyst.[51] A conversion of MP ~95% and S-CP of *ca.* 75% are reported over these catalysts. Bondareva *et al.*[15] applied phosphorus modified V_2O_5–TiO_2 catalysts for the ammoxidation of MP and reported that the content of P in the total catalyst plays a key role on the performance. The active sites of the samples with a low concentration of phosphorus contain V^{5+} cations in a strongly distorted octahedral oxygen environment, which are strongly bound to a support due to the formation of V–O–Ti bonds. The catalytic properties of the samples containing high P_2O_5 contents (10 wt%) are due to the presence of a triple V–P–Ti compound with an atomic ratio of V : P : Ti that is nearly 1 : 1 : 1. The V^{5+} cations in this compound with high P contents are present in a weakly distorted tetrahedral oxygen environment and are bound to the tetrahedral P^{5+} cations. The authors studied two regions of compositions such as the catalysts with low (<5 wt% P_2O_5) and high (>10 wt% P_2O_5) contents of the P additive. The low content of P increases the activity, while the high content of P decreases both the activity as well as selectivity of the desired product, accompanied by a simultaneous increase in the selectivities of byproducts such as pyrazine and carbon oxides. On the other hand, addition of alkali promoters, *e.g.* Na- or K-modified V_2O_5/TiO_2 catalysts in MP ammoxidation, showed reduced activity and selectivity of the catalysts due to formation of bronzes (*e.g.* MV_6O_{15}) and vanadates (*e.g.* α-$NaVO_3$, $K_3V_5O_{14}$ *etc.*).[25] However, the active sites of these modified samples are reported to be similar to those in the binary V–Ti–O catalysts, *i.e.* V^{5+} cations strongly bound to TiO_2 and located in a distorted octahedral oxygen environment. The higher the content and basicity of the additive, the more pronounced is the decrease in the V/Ti ratio and the activity. In another study, Bondareva *et al.*[3] investigated the mechanism of ammoxidation of MP by *in situ* FTIR and described that the interaction of methylpyrazine with the catalyst surface involves a consecutive transformation of coordinatively bound methylpyrazine into oxygenated surface compounds, *e.g.* an aldehyde-like complex and an asymmetrical carboxylate species, which are also coordinatively bound through the nitrogen atom to the surface Lewis acid sites. In the presence of ammonia, such oxy-intermediates further interact with adsorbed ammonia species and form surface amidopyrazine and cyanopyrazine products.

In the last part, we would like to give a brief summary of different catalytic systems applied, reaction conditions, and space–time yields reported by various research groups and compare them with that of the present metal vanadates. For instance, heteropoly acids, *e.g.*,[5] $FePO_4$ (ref. 20), gave a MP conversion of 75–80%, CP yield of 50–56% and STY of only 65–135 $g_{CP}\ kg_{cat}^{-1}\ h^{-1}$. More than 80% yield of CP at 99% conversion of MP was also reported on β-$VOPO_4/SiO_2$ (ref. 52) and $VSbPO_x$ (ref. 53) catalysts, but the STY of CP achieved over these systems is relatively low, *i.e. ca.* 110 $g_{CP}\ kg_{cat}^{-1}\ h^{-1}$. One US patent claims 87% conversion of MP, 67% yield of CP with very low STY of CP (~75 $g_{CP}\ kg_{cat}^{-1}\ h^{-1}$) using a multicomponent $MoPWAlO_x$ catalyst at a high reaction temperature of 440 °C.[54] To the best of our knowledge, the best STY of CP reported so far in the literature is <150 $g_{CP}\ kg_{cat}^{-1}\ h^{-1}$. On the whole, it can be stated that the present metal vanadate catalysts showed much improved catalytic performance in terms of atom efficiency and space–time yields of CP.

4. Summary and conclusions

The results revealed clearly that the Nb/V ratio in $NbVO_x$ solids is indeed an important parameter that needs to be tuned carefully for improving the oxidation properties of solids in a more selective way. The change in the Nb/V ratio has shown a substantial influence on the physico-chemical

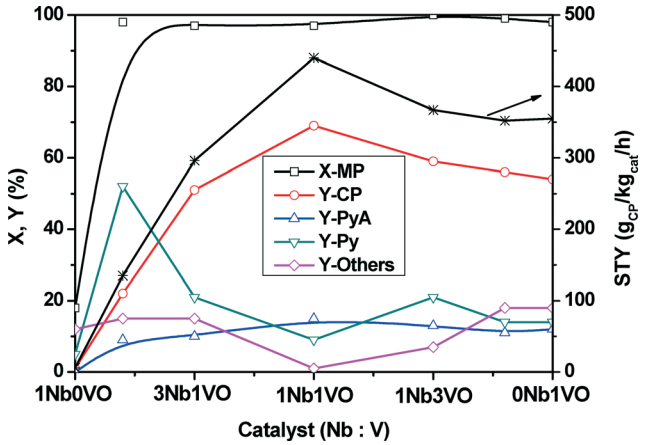

Fig. 9 A comparison of conversion of MP, product yields and selectivity as well as space–time yields of CP obtained over different Nb–V–O catalysts at 380 °C (reaction conditions: MP : H_2O : NH_3 : air : N_2 = 1 : 13 : 7 : 26 : 22; cat. wt. 1 g; MP = methylpyrazine, CP = cyanopyrazine, Py = pyrazine, PyA = pyrazinamide).

characteristics (*e.g.* porosity, phase composition, crystallinity, nature of VO_x species, reducibility, surface composition, morphology *etc.*) of the catalysts and thereby catalytic activity and selectivity as well. In the present study, the catalytic properties of Nb–V–O solids were evaluated for the ammoxidation of MP to CP. Surface areas and pore volumes were found to decrease with the dropping Nb/V ratio of the solids. Moreover, the type of VO_x species formed and the crystalline phases present in the calcined solids were observed to depend strongly on the content of vanadium (*i.e.* Nb/V ratio) in the catalyst. The XPS analysis exhibited a clear enrichment of vanadium in the near-surface region in the best catalyst (Nb/V = 1), which appeared to be responsible for an enhanced selectivity of CP. The catalytic results demonstrated that the ratio of Nb/V in the final catalyst played a key role on the catalytic performance. The results showed that the nature of the vanadium–oxygen sites changed with vanadia content, too. The oligomeric/polymeric vanadia species were considered to be selective for the formation of CP during the ammoxidation of MP. Among all the catalysts tested, the best performance was achieved over the catalyst having an Nb/V ratio of 1 (which corresponds to the $NbVO_5$ phase). Furthermore, almost a total conversion of MP and *ca.* 70% yield of CP (close to 90% for aggregated yield of CP and PyA) along with extremely high space–time yield of CP (440 g_{CP} kg_{cat}^{-1} h^{-1} or 600 g_{CP+PyA} kg_{cat}^{-1} h^{-1}) was successfully achieved. Finally, the conclusion is that 1Nb1VO ($NbVO_5$) is the best composition for delivering the high productivity of the desired product (CP). This might be due to the involvement of all Nb^{5+} and V^{5+} ions in the bond formation of Nb–V–O oxide, and also due to the surface enrichment of vanadium species as a VO_4^{3-}.

Acknowledgements

Dr. M. Schneider and Dr. J. Radnik both of LIKAT are thanked for XRD and XPS measurements.

References

1 A. Martin and V. N. Kalevaru, *ChemCatChem*, 2010, **2**, 1504–1522.
2 A. Kagarlitskii, L. Krichevskii and A. Amirkhanova, *Pharm. Chem. J.*, 1999, **33**, 381–383.
3 V. M. Bondareva, T. V. Andrushkevich, E. A. Paukshtis, N. A. Paukshtis, A. A. Budneva and V. N. Parmon, *J. Mol. Catal. A: Chem.*, 2007, **269**, 240–245.
4 V. M. Bondareva, T. V. Andrushkevich, O. B. Lapina, A. A. Vlasov and L. S. Dovlitova, *React. Kinet. Catal. Lett.*, 2003, **79**, 165–173.
5 N. Lingaiah, K. M. Reddy, P. Nagaraju, P. S. Sai Prasad and I. E. Wachs, *J. Phys. Chem. C*, 2008, **112**, 8294–8300.
6 P. Nagaraju, N. Lingaiah, M. Balaraju and P. S. Sai Prasad, *Appl. Catal., A*, 2008, **339**, 99–107.
7 Global Tuberculosis Report of WHO, 2012.
8 I. E. Wachs, *Catal. Today*, 2005, **100**, 79–94.
9 E. Heracleous and A. A. Lemonidou, *J. Catal.*, 2010, **270**, 67–75.
10 G. V. Isaguliants and I. P. Belomestnykh, *Catal. Today*, 2005, **100**, 441–445.
11 J. M. Amarilla, B. Casal and E. Ruiz-Hitzky, *J. Mater. Chem.*, 1996, **6**, 1005–1011.
12 Z. Zhao, X. Gao and I. E. Wachs, *J. Phys. Chem. B*, 2003, **107**, 6333–6342.
13 F. Barbieri, D. Cauzzi, F. De Smet, M. Devillers, P. Moggi, G. Predieri and P. Ruiz, *Catal. Today*, 2000, **61**, 353–360.
14 J. Holmberg, R. Häggblad and A. Andersson, *J. Catal.*, 2006, **243**, 350–359.
15 V. M. Bondareva, T. V. Andrushkevich, O. B. Lapina, D. F. Khabibulin, A. A. Vlasov, L. S. Dovlitova and E. B. Burgina, *Kinet. Catal.*, 2004, **45**, 104–113.
16 C. Hong and Y. Li, *Chin. J. Chem. Eng.*, 2006, **14**, 670–675.
17 K. Mohan Reddy, N. Lingaiah, K. N. Rao, P. Nagaraju, P. S. Sai Prasad and I. Suryanarayana, *Catal. Lett.*, 2009, **130**, 154–160.
18 Ch. Srilakshmi, N. Lingaiah, P. Nagaraju, P. S. Sai Prasad, K. V. Narayana, A. Martin and B. Lücke, *Appl. Catal. A*, 2006, **309**, 247–253.
19 K. N. Rao, K. M. Reddy, N. Lingaiah, I. Suryanarayana and P. S. Sai Prasad, *Appl. Catal. A*, 2006, **300**, 139–146.
20 P. Nagaraju, Ch. Srilakshmi, N. Pasha, N. Lingaiah, I. Suryanarayana and P. S. Sai Prasad, *Appl. Catal. A*, 2008, **334**, 10–19.
21 P. Nagaraju, Ch. Srilakshmi, N. Pasha, N. Lingaiah, I. Suryanarayana and P. S. Sai Prasad, *Appl. Catal. A*, 2008, **334**, 10–19.
22 B. Manohar, *J. Chem. Pharm. Res.*, 2012, **4**, 2781–2788.
23 Ch. Srilakshmi, P. Nagaraju, B. Sreedhar, P. S. Saiprasad, V. N. Kalevaru, B. Lücke and A. Martin, *Catal. Today*, 2009, **141**, 337–343.
24 B. M. Reddy, B. Manohar, E. P. Reddy, K. S. Patil and A. V. Ramarao, *Ind. Pat.* 182 185 A1, 1999, CSIR, New Delhi, India.
25 V. M. Bondareva, T. V. Andrushkevich, O. B. Lapina, A. A. Vlasov, L. S. Dovlitova and E. B. Burgina, *React. Kinet. Catal. Lett.*, 2003, **78**, 355–363.

26 L. Forni, *Appl. Catal.*, 1988, **37**, 305–314.
27 E. Rojas, M. O. Guerrero-Pérez and M. A. Bañares, *Catal. Commun.*, 2009, **10**, 1555–1557.
28 M. O. Guerrero-Pérez and M. A. Bañares, *Catal. Today*, 2009, **142**, 245–251.
29 C. Lucarelli, P. Moggi, F. Cavani and M. Devillers, *Appl. Catal. A*, 2007, **325**, 244–250.
30 N. Krins, L. Lepot, R. Cloots and B. Vertruyen, *Solid State Ionics*, 2009, **180**, 848–852.
31 N. Ballarini, F. Cavani, C. Cortelli, C. Giunchi, P. Nobili, F. Trifirò, R. Catani and U. Cornaro, *Catal. Today*, 2003, **78**, 353–364.
32 A. Polte and H. Langbein, *Z. Anorg. Allg. Chem.*, 1994, **620**, 1947–1952.
33 N. Dhachapally, V. N. Kalevaru and A. Martin, *Eur. Pat.* 2428267 A1, LIKAT, Rostock, Germany, 2012.
34 N. Dhachapally, V. N. Kalevaru, J. Radnik and A. Martin, *Chem. Commun.*, 2011, **47**, 8394–8396.
35 N. Dhachapally, V. N. Kalevaru, A. Brückner and A. Martin, *Appl. Catal. A*, 2012, **443–444**, 111–118.
36 A. V. Rosario and E. C. Pereira, *J. Solid State Electrochem.*, 2005, **9**, 665–673.
37 Y. Zhao, X. Zhou, L. Ye and S. C. E. Tsang, *Nano Rev.*, 2012, **3**, 17631–17642.
38 C. Sangwichien, G. L. Aranovich and M. D. Donohue, *Colloids Surf., A*, 2002, **206**, 313–320.
39 F. Rouquerol, J. Rouquerol and K. Sing, Adsorption by Powders and Porous Solids Principles, *Methodology and Applications*, Academic Press, San Diego, CA, 1999.
40 H. Berndt, A. Martin, A. Brückner, E. Schreier, D. Müller, H. Kosslick, G. U. Wolf and B. Lücke, *J. Catal.*, 2000, **191**, 384–400.
41 H. Tian, I. E. Wachs and L. E. Briand, *J. Phys. Chem. B*, 2005, **109**, 23491–23499.
42 Z. Zhao, Y. Yamada, Y. Teng, A. Ueda, K. Nakagawa and T. Kobayashi, *J. Catal.*, 2000, **190**, 215–227.
43 N. Kumagai, N. Ikenoya, I. Ishiyama and K. Tanno, *Solid State Ionics*, 1988, **28–30**, 862–867.
44 M. Amarilla, B. Casal, J. C. Galvan and E. Ruiz-Hitzky, *Chem. Mater.*, 1992, **4**, 62–67.
45 G. Silversmit, D. Depla, H. Poelman, G. B. Marin, R. De Gryse and J. Electron, *J. Electron Spectrosc. Relat. Phenom.*, 2004, **135**, 167–175.
46 M. Demeter, M. Neumann and W. Reichelt, *Surf. Sci.*, 2000, **454–456**, 41–44.
47 H. Najjar and H. Batis, *Appl. Catal. A*, 2010, **383**, 192–201.
48 O. S. Owen and H. H. Kung, *J. Catal.*, 1993, **79**, 265–284.
49 M. A. Chaar, D. Patel, M. C. Kung and H. H. Kung, *J. Catal.*, 1987, **105**, 483–498.
50 D. Patel, P. J. Andersen and H. H. Kung, *J. Catal.*, 1990, **125**, 132–142.
51 G. Centi, *Appl. Catal. A*, 1996, **147**, 267–298.
52 S. Shimizu, T. Shoji, N. Abe, M. Doba, A. Taguro, A. Iguchi and T. Nakaishi, US 4 778 890, 1988, Koei Chemical Co. Ltd., Japan.
53 S. Shimizu, T. Shoji, N. Abe, M. Doba, A. Taguro, A. Iguchi and T. Nakaishi, EP 253 360 B1, 1988, Koei Chemical Co. Ltd., Japan.
54 S. Shimizu, T. Shoji, K. Kono and T. Nakaishi, US 4 931 561, 1990, Koei Chemical Co. Ltd., Japan.

